This article has been accepted for publication in a future issue of this journal, but has not been fully edited. Content may change prior to final publication. Citation information: DOI 10.1109/TMECH.2020.3037303, IEEE/ASME Transactions on Mechatronics

Compliant Bistable Grippers Enable Passive Perching for Micro Aerial Vehicles

Haijie Zhang, Elisha Lerner, Bo Cheng, and Jianguo Zhao

***Abstract*—Micro aerial vehicles (MAV) with multiple rotors, or multicopters, have many promising applications ranging from environmental monitoring, agricultural inspection, to package delivery. These applications, however, usually face a critical problem: the flight time of MAVs is limited due to the low aerodynamic efficiency and high energy consumption. One promising solution is to make them rest on desired objects using perching, an important capability in biological flyers (e.g., birds). In this paper, we present the design and experimentation of a novel perching mechanism: a low cost, 3D printed gripper with bistability (i.e., two stable states). The gripper has two unique characteristics. First, using bistability, it can passively switch from open to closed state using the impact between the gripper and the perching object, alleviating the requirement for precise motion control. Second, the gripper has two perching methods for different objects. For objects with a small height, it can form a closed diamond shape to encircle the objects (encircling method). For objects with a large height, the gripper's two fingers can clip on each side of the objects to utilize the friction forces for perching (clipping method). We analyze the proposed gripper design to predict the required force for opening and closing the gripper. We also predict the size of objects that will allow for successful perching for the clipping method. All the theoretical analyses are experimentally verified. Finally, we integrate the gripper onto a palm-size quadcopter to enable a mechatronic system for perching, and demonstrate successful perching with both clipping and encircling methods as well as aerial grasping. Although our bistable gripper is used with a palm-size quadcopter, the design strategy can also be applied to large-size MAVs for both energy efficient perching and aerial grasping.**

***Index Terms*—Perching, bistable mechanism, aerial grasping, micro aerial vehicles**

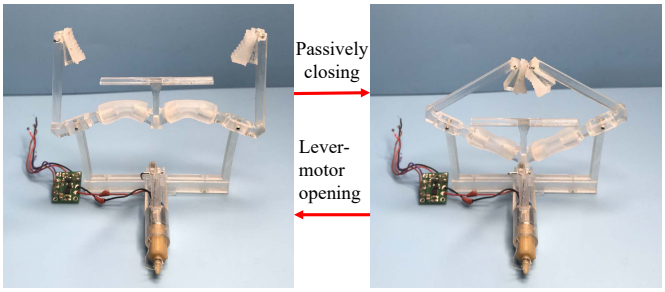

(a) Proposed bistable gripper with two stable states

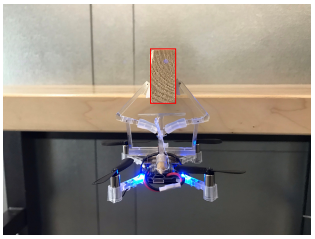

(b) Clipping perching

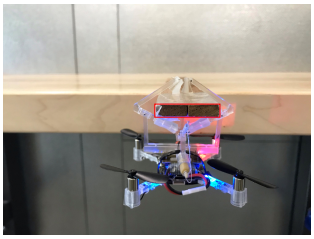

(c) Encircling perching

Fig. 1. Proposed bistable gripper. (a) the two stable states of the gripper, which can switch from open to closed state through impact force, and from closed to open using a lever-motor system. (b) the clipping perching method utilizes the friction force to hold the robot's weight. (c) the encircling perching method relies on a closed diamond shape formed by the fingers to hold the robot's weight.

I. Introduction

RECENT years have witnessed the growing popularity of Micro Aerial Vehicles (MAVs) in recreational, scientific, and military applications. However, MAVs, especially those with multiple rotors, are facing a common critical problem: limited flight time. As the aerodynamic efficiency and energy storage capability decrease with flyers' scale, the flight time for commercial MAVs is usually less than 30 minutes [1]. One promising solution is to learn from biological flyers to perch onto desired objects [2]. Similar to biological flyers that can rest and feed after perching, MAVs can also perch to maintain a desired height and orientation to inspect, monitor, or even recharge. In this case, perching can significantly extend MAVs' functioning time for long-duration monitoring tasks since the energy required after perching is minimal compared with the energy for staying airborne [3].

However, it's challenging to accomplish robust perching. Recent studies on insects and birds suggest that successful perching needs to synergistically integrate two types of intelligence: computational and mechanical [2], [4]. Computational intelligence involves the estimation, planning, and control for the perching motion, which can detect the perching object, estimate the flight state (e.g., velocities, orientations), plan proper trajectories, and control the motion, all of which should be conducted accurately and rapidly given the stringent time due to the fast motion during perching [5], [6]. Mechanical intelligence involves the special mechanical aspects for legs that can be leveraged to damp out landing impact and allow for firm grip onto the desired objects. This intelligence is critical in alleviating the requirement for computational intelligence, especially for flyers with limited computational capability (e.g., fruit flies). In this paper, we present a novel perching mechanism design with mechanical intelligence that allows passively perching without accurate control of the contact speed, thereby reducing the requirement for computational intelligence.

Haijie Zhang, Elisha Lerner, and Jianguo Zhao are with the Department of Mechanical Engineering at Colorado State University, Fort Collins, CO, 80523, USA

Bo Cheng is with the Department of Mechanical Engineering, Pennsylvania State University, University Park, PA, 16802, USA.

1083-4435 (c) 2020 IEEE. Personal use is permitted, but republication/redistribution requires IEEE permission. See http://www.ieee.org/publications_standards/publications/rights/index.html for more information.
Authorized licensed use limited to: COLORADO STATE UNIVERSITY. Downloaded on July 26,2021 at 17:17:17 UTC from IEEE Xplore. Restrictions apply.

This article has been accepted for publication in a future issue of this journal, but has not been fully edited. Content may change prior to final publication. Citation information: DOI 10.1109/TMECH.2020.3037303, IEEE/ASME Transactions on Mechatronics

Many perching mechanisms or methods have been recently investigated. Here we briefly review several recent ones (a detailed review can be found in [3], [7]). Based on the perching objects, we can categorize most perching methods into surface perching and rod perching. Surface perching means the perching object is a flat surface such as a wall or a ceiling, while rod perching means the object resembles a rod shape (e.g., tree branches). *For surface perching,* adhesion pad and microspine are widely used. For instance, electrostatic adhesion is adopted in [8] to perch and detach the Robobee on surfaces with different materials. Anderson controlled a fixed-wing MAV to adhere itself to a perching surface with a sticky pad [9]. A perching mechanism using fiber-based dry adhesives and a passive self-alignment system is implemented on a 300 g flying platform [10]. Kovač *et al.* presented a 4.6 g perching mechanism that could convert the impact into the snapping motion to stick needles into the surface [11]. Recently, they also proposed a spider inspired tensile anchoring modules to launch several tensile anchors on fixed objects to perch the MAV [12]. Mehanovic *et al.* proposed a bird-like pitch up strategy for a fix-wing drone to decrease the impact force and adjust the perching orientation [13]. Using gecko-inspired adhesive grippers, Thomas *et al.* controlled a MAV to perch on inclined surfaces [14]. Stanford Climbing and Aerial Maneuvering Platform (SCAMP) was developed for perching, climbing, and taking off again [7]. *For rod perching*, a perching mechanism with grasping capability is usually adopted. For instance, a songbirds-inspired perching mechanism utilizes the weight of MAV to passively apply tendon tension to actuate the gripping foot [15]. Nguyen *et al.* designed a passively adaptive microspine grapple that could conform to the surface of convex perching targets such as tree branches [16]. Hang *et al.* designed a set of actuated landing gears which enables MAVs to perch or rest on many different objects [17].

In this paper, we present a novel mechanism for rod perching: a bistable gripper that can switch between a stable open state and another stable closed state (Fig. 1(a)). Such a gripper has two advantages for perching compared with existing methods [7]. On one hand, it can passively close the gripper by directly using the impact force during perching instead of an actuator. Consequently, it can alleviate the requirement for computational intelligence since we don't need to precisely control the contact speed: As long as the speed is in a range to generate a sufficient impact force for switching the state, the perching process will succeed. On the other hand, the gripper can maintain the stable states without additional energy input, meaning that it can hang on a perching object without consuming energy, which makes it promising for applications requiring long-duration monitoring.

Bistable mechanisms have been widely used in different areas [18]. For grippers, Nguyen *et al.* designed a bistable gripper for grasping and releasing objects [19]. Thuruthel *et al.* [20] designed a soft bistable gripper to rapidly grasp unstructured objects. Besides grippers, various mechanical structures with bistability have also been recently exploited for many applications including deployable structures [21], jumping robots [22], swimming robots [23], origami robots [24], soft robots [25], shape morphing [26], mouse trap [27], and mechanical metamaterials [28]. To the best of our knowledge, however, it has yet to see how bistability can be used for perching mechanisms except our recent work [29].

In our previous research [29], we designed a bistable gripper (we will use old bistable gripper to distinguish it from the new one presented in this paper) with three-fingers as a mechanism for rod perching. Installed on top of the MAV, the gripper can switch from open to closed state using the impact force between the gripper and the perching object. When the gripper closes, its three fingers can form a closed area to hang the MAV. To release from the perching object, resistance wires are used to heat the plastic fingers to open the gripper.

The new gripper presented in this paper (Fig. 1(a)) is substantially improved from the old one. Specifically, we redesign the gripper to a two-finger structure instead of three-finger, which improves the rate of successful perching and decreases the weight of the gripper. We also enable a new perching method: clipping (Fig. 1(b)) in addition to our previous encircling method (Fig. 1(c)), by appending the upper part of the two fingers with soft pads to generate large friction forces on surfaces. We have also added a motor-driven lever system to open the gripper, which is more repeatable compared to our previous heating based method.

There are three major contributions in this paper. First, we utilize the concept of bistability to design a novel gripper, which suits MAV perching well since it can rely on impact forces to trigger the perching process, and does not require additional energy after perching. Second, we thoroughly analyze the bistability of the mechanism to generate a design guideline for selecting proper design parameters, which can be applied to design other bistable grippers for perching or aerial grasping with larger-scale MAVs. Third, we develop a complete mechatronic system for aerial perching and grasping by integrating the gripper onto a palm-size quadcopter, which can perform repeatable perching and releasing.

The rest of this paper is organized as follows. Section II introduces the working principle of bistable mechanisms and the new gripper design. Section III analyzes the mechanism by deriving the equation for force-displacement characteristic and equation for grasping forces of the bistable gripper. The bistability of the gripper based on two important parameters is also discussed. Section IV details the experiment setup and results to verify the force-displacement characteristic modeling and demonstrates the repeatable perching-releasing cycle for two different perching methods. Section V summarizes the paper and outlines future work.

II. Bistable gripper design

Our gripper design is based on a basic bistable mechanism as shown in Fig. 2. The mechanism consists of four revolute joints, two rigid links, a switching pad, and two beams connected to a rigid base. It has two stable configurations illustrated as S_1 and S_2, where no force input is needed to maintain the configuration. It can switch between S_1 and S_2 through external forces. For instance, it can switch from S_1 to S_2 when a force F is applied upward on the switching

1083-4435 (c) 2020 IEEE. Personal use is permitted, but republication/redistribution requires IEEE permission. See http://www.ieee.org/publications_standards/publications/rights/index.html for more information.
Authorized licensed use limited to: COLORADO STATE UNIVERSITY. Downloaded on July 26,2021 at 17:17:17 UTC from IEEE Xplore. Restrictions apply.

This article has been accepted for publication in a future issue of this journal, but has not been fully edited. Content may change prior to final publication. Citation information: DOI 10.1109/TMECH.2020.3037303, IEEE/ASME Transactions on Mechatronics

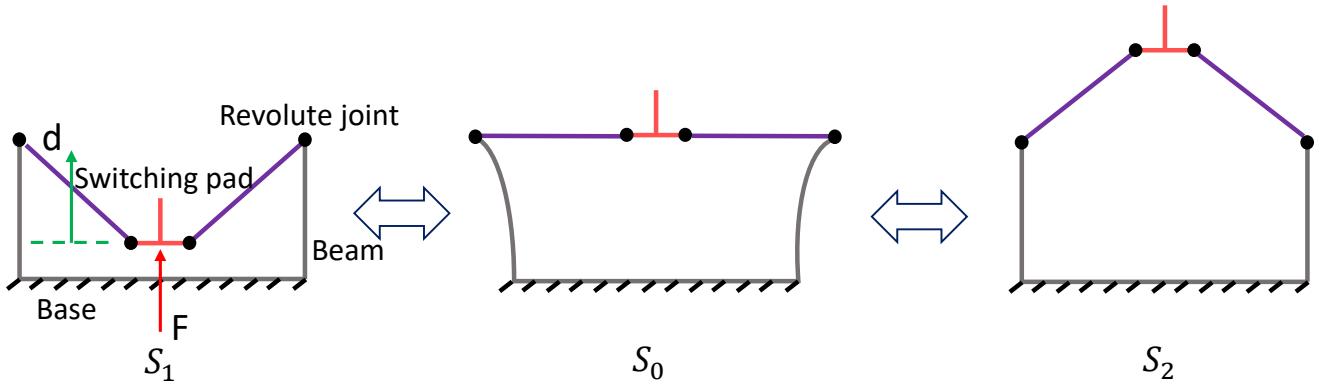

Fig. 2. Schematic of a basic bistable mechanism for our bistable gripper. It has four revolute joints in black, two rigid links in purple, a switching pad in pink, and two beams (together with the base) in grey. It has two stable states at S_1 and S_2. When an upward force F is applied on the switching pad, the mechanism can switch from S_1 to S_2 through the intermediate state S_0. During the process, the two vertical beams will be pushed outside. If the force is removed, it can switch to the closest stable state S_1 or S_2 with the recovery forces generated from bending beams. And vice versa, a large enough downward force on the switching pad can make the mechanism switch from S_2 to S_1 through S_0.

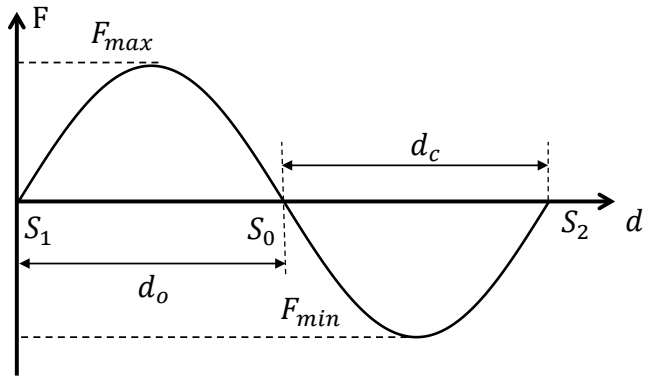

Fig. 3. Force-displacement characteristic for the basic bistable mechanism. The figure shows the force required to maintain the switching pad at a specific travel distance. The maximum force for this transition from S_1 to S_2 is F_{max} and the minimum force is F_{min}. The displacement the switching pad needs to travel is d_o from S_1 to S_0 and d_c from S_0 to S_2.

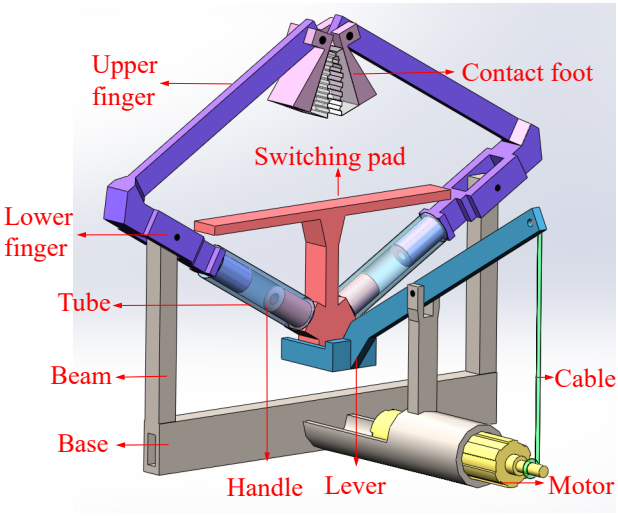

Fig. 4. Solid model for bistable gripper in the closed stable state. The gripper consists of a base with beams, fingers, a switching pad, contact feet, tubes, and a lever-motor releasing system. One side of the lever can be dragged by the motor while the other side will push the bottom of the switching pad upward to open the gripper.

pad. During the process, the rigid links will rotate, and the two beams will be bent outside. When it arrives configuration S_0, no force is needed to maintain the current unstable state. After passing S_0, an opposite force is required to maintain the current configuration. Otherwise, it can switch to S_2 with the recovery force from bending beams. And vice versa, a downward force can also be applied on the switching pad to make the mechanism switch from S_2 to S_1 through S_0. The relationship between the force F and displacement d is called force-displacement characteristic as shown in Fig. 3. In the figure, we have two critical forces: the maximum force F_{max} and the minimum force F_{min}, meaning the force needs to be larger than F_{max} to switch from S_1 to S_2, larger than $|F_{min}|$ to switch from S_2 to S_1. d_o and d_c are the corresponding displacements between two neighboring zero forces.

Our new design is based on the basic bistable mechanism (Fig. 2) with a key difference: the basic mechanism has a symmetric force-displacement characteristic (i.e., $F_{max} = |F_{min}|$), but our bistable gripper can have a tunable force-displacement profile with different magnitudes of F_{min} and F_{max} that can deal with the requirements of perching: easy to close (a small impact force can close the gripper), and stable to hold (only a large force can open the gripper). Such tunable performance is accomplished by replacing the two revolute joints attaching to the switching pad with elastic/compliant joints. Details on why such a change can lead to tunable performance are elaborated in section III-C.

Our new design can be illustrated using a solid model (Fig. 4). It consists of the following elements: a base with two vertical beams, two fingers (consisting of lower finger and upper finger) connected to the beams via rotational joints, a switching pad that will contact the perching object to close and be pushed by the lever to open, two contact feet attached to the end of the two upper fingers, two elastic tubes connecting the fingers to the switching pad, and a cable-driven lever actuated by a DC motor. We choose tubes as compliant joints instead of traditional torsional springs since tubes can be easily

1083-4435 (c) 2020 IEEE. Personal use is permitted, but republication/redistribution requires IEEE permission. See http://www.ieee.org/publications_standards/publications/rights/index.html for more information.
Authorized licensed use limited to: COLORADO STATE UNIVERSITY. Downloaded on July 26,2021 at 17:17:17 UTC from IEEE Xplore. Restrictions apply.

This article has been accepted for publication in a future issue of this journal, but has not been fully edited. Content may change prior to final publication. Citation information: DOI 10.1109/TMECH.2020.3037303, IEEE/ASME Transactions on Mechatronics

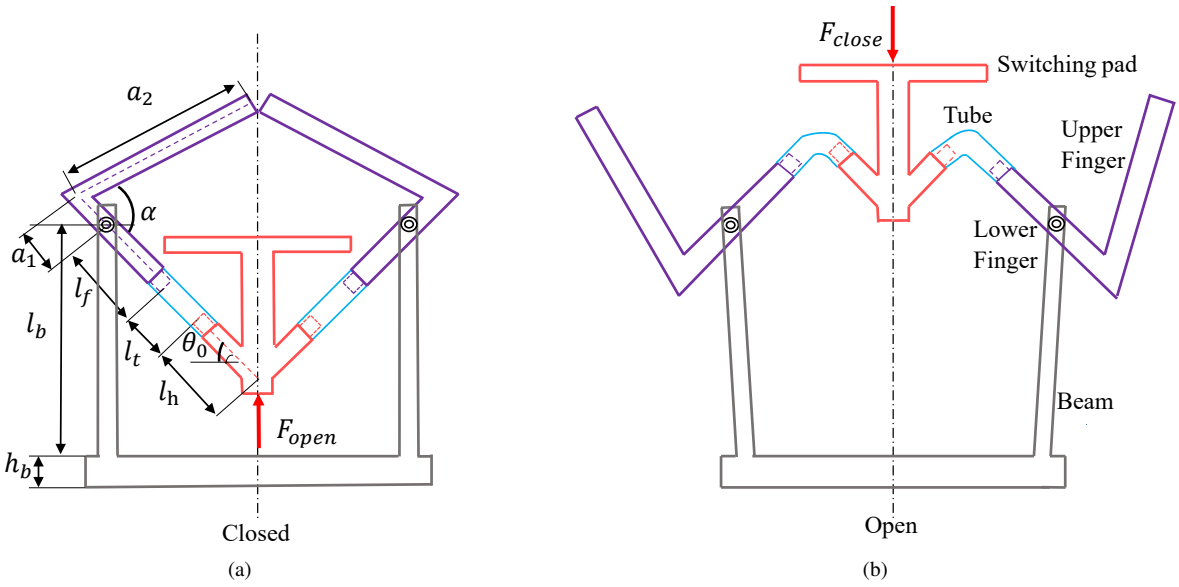

Fig. 5. The schematic of the bistable gripper in two stable states: The left figure is the closed state, where no strain energy is in the tubes or beams. A force F_{open} can be applied on the bottom of the switching pad to open it. The right figure is the open state, where strain energy is stored in both beams and tubes with beams being pushed outward and tubes being bent. A force F_{close} can be applied on the top of the switching pad to close it. Some unnecessary parts such as the contact feet and lever-motor system are not shown for simplicity .

customized to different lengths to generate different torsional stiffness. Also, the tubes are chosen as the compliant joints for convenient fabrication [30], but it can be replaced with any compliant materials (e.g., multimaterial 3D printing [31]).

With such a design, the gripper has a closed stable state and an open stable state as shown in Fig. 1(a). It can switch from the initially closed state to the open state as follows. If an upward force from the cable-driven lever is applied on the bottom of the switching pad, the two fingers will pivot around the rotational joints to push the two vertical beams outward and bend the two tubes, storing strain energy in the beams and tubes. When the switching pad passes a critical point, the stored strain energy will push the switching pad upward without any input. Eventually, the gripper will stop at the open stable state. Similarly, the gripper can switch from the open state to the closed state by applying a downward force on the top of the switching pad. For perching, this force can directly come from the impact force.

Compared with our old gripper [29], we revised the design in three major aspects. First, the old gripper has three beams on the base and three fingers rotating on each beam. Although the three fingers can form a closed shape to hang on a perching object, they complicate the perching preparation of the old gripper since the MAV needs a good yaw angle to initiate the perching. Only in the desired range for the yaw angle could the fingers grab the perching object successfully. To address this issue, we use only two fingers rotating on two beams in the new design. Such a design can increase the range of perching yaw angle for about 60°. Second, besides the encircling perching method that the old gripper utilizes, the new gripper can also perch with a new clipping method for large objects that the gripper cannot encircle. As shown in Fig. 1(b), when the new gripper is closed, the two feet can contact the two sides of the object to generate friction forces to clip on the object. To generate large enough friction forces, each foot is composed of a soft film made from elastomers glued onto a rigid base, which can freely rotate about the upper finger. With the rotational feet, the gripper can adapt to different shaped objects in natural environments. Third, we design a new lever-motor system to open the new gripper to release the MAV from the perching state. In the old gripper, the releasing mechanism is based on heat and not repeatable. As shown in Fig. 4, the new lever-motor system consists of a level driven by a motor through a cable. One side of the lever is connected to a motor shaft through a cable, while the other side is under the switching pad. After opening, the motor will be controlled to rotate in the opposite direction to release the cable, and the lever will switch back to the original position due to the heavier switching side.

III. Bistable Gripper Analysis

To use the designed gripper for perching, we need to analyze the relationship between the force applied to the switching pad and the resulting displacement: the force-displacement characteristic. Such a relationship can determine the required force to switch between the two stable states. After that, we derive the friction force that can be generated by the gripper for clipping perching. In the end, we investigate the underlying working principle and show how the design parameters will influence the mechanism's bistability by defining a bistability index.

A. Force-displacement characteristic

To analyze the force-displacement characteristic, we redraw a simplified sketch of the new gripper in Fig. 5 for both open and closed state. Since the lever-motor system does not influence the force-displacement characteristic, it is not drawn

1083-4435 (c) 2020 IEEE. Personal use is permitted, but republication/redistribution requires IEEE permission. See http://www.ieee.org/publications_standards/publications/rights/index.html for more information.
Authorized licensed use limited to: COLORADO STATE UNIVERSITY. Downloaded on July 26,2021 at 17:17:17 UTC from IEEE Xplore. Restrictions apply.

This article has been accepted for publication in a future issue of this journal, but has not been fully edited. Content may change prior to final publication. Citation information: DOI 10.1109/TMECH.2020.3037303, IEEE/ASME Transactions on Mechatronics

in the sketch. As shown in Fig. 5, l_h is the distance from the end of the switching pad handle to the centerline of the switching pad. l_t is the length of the hollow tube. l_f is the distance from the pivot to the end of the lower finger. a_2 is the upper finger's length, while a_1 is the length from the centerline of the upper finger to the pivot. The angle between the upper and lower finger is α. The distance from the pivot to the base is l_b. The angle between the handle of the switching pad and the horizontal direction is θ_0. h_b is the height of the base.

The bistability is generated by the deformation of the elastic tube and the vertical beam (see section III-C for a detailed analysis). Therefore, we will model the statics for the gripper by considering these two elements. For the flexible tube, we model it with the PRBM [18], a widely used technique for compliant mechanisms. Specifically, we model the tube as two rigid links connected by a rotational joint. Note that there are more complicated models with more joints [31] as well as models with Beam Constraint Model (BCM) which takes into account the nonlinearities arising from load equilibrium applied in the deformed configuration [32], but we use the PRBM for simplicity. To represent the tube's resistance to bending, we assume a torsional spring associated with the joint. The joint locates at γl_t away from the end connected with the fingers, where l_t is the tube length. Detailed γ values can be found in [18]. In this paper, we use $\gamma = 0.83$ to maximize the pseudo-rigid-angle while achieve an accurate estimation [18]. The spring constant for the torsional spring is $k_\theta = \pi\gamma^2 E_{yt} I_t / l_t$, where E_{yt} and I_t are Young's modulus and second moment of inertia of the tube, respectively. For the beam, we model it as a linear spring which can only be compressed in the horizontal direction, since its outward displacement is small. The spring constant is $k_d = 3E_{yb}I_b/l_b^3$, where E_{yb} and I_b are Young's modulus and second moment of inertia of the beam, respectively. We ignore the change of l_b in vertical direction since the change is estimated to be only 0.63% of the original beam length in our design.

With the above models for tubes and beams, Fig. 5 can be redrawn in Fig. 6 for mathematical derivation. The green lines represent the initial closed configuration C_0, and the red lines represent one of the configurations during state transition C_1. Due to the symmetry of the gripper, the switching pad at the centerline can only move in the vertical direction with displacement d.

Since the applied force F is the only input and the switching process is quasi-static, the force-displacement characteristic between F and d can be derived from the total strain energy E in linear springs for beams and torsional springs for tubes through the following equation [23]:

$$F = \frac{\partial E}{\partial d} \tag{1}$$

From the assumptions about linear and torsional springs, the strain energy in the two beams can be written as

$$E_b = k_d {d_b}^2$$

where d_b is the horizontal displacement of the linear spring. It can be solved from the following geometrical relationship

$$H^2 + {L_0}^2 = (H-d)^2 + (L_0 + d_b)^2$$

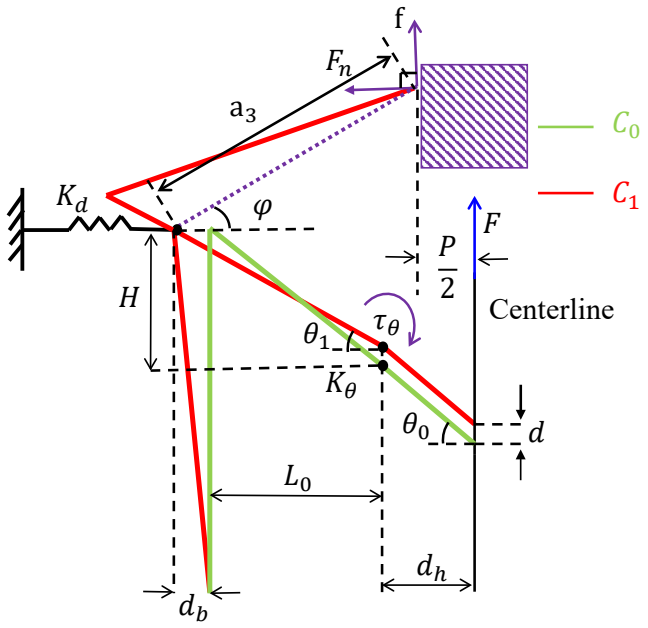

Fig. 6. Sketch for mathematical modeling of the gripper. Only the left part of the gripper is shown. The bending beam is modeled as a linear spring, and the tube is modeled as a torsional spring. The green lines represent the initial closed state C_0 and red lines represent one of the configurations during state transition C_1. For clarity, the upper fingers are not drawn in C_0. For the clipping scenario, a purple rectangle is drawn as the perching object and normal force F_n and friction force f are drawn in purple at the contact point.

where $L_0 = (l_f + \gamma l_t)\cos\theta_0$, $H = (l_f + \gamma l_t)\sin\theta_0$ are constants (Fig. 6). With this equation, we can solve d_b as a function of d: $d_b = \sqrt{2Hd + {L_0}^2 - d^2} - L_0$. The strain energy in the two tubes can be written as

$$E_t = k_\theta(\theta_1 - \theta_0)^2$$

where θ_1 is the angle between the lower finger and the horizontal axis at configuration C_1, which can also be represented as a function of d: $\theta_1 = \arctan(H-d)/(L_0 + d_b)$. Therefore, the total strain energy E is

$$E = E_t + E_b = k_\theta(\theta_1 - \theta_0)^2 + k_d {d_b}^2 \tag{2}$$

Plugging the energy into equation (1), we can obtain the force-displacement characteristic as

$$F(d) = -\frac{2}{L_0 + d_b}\left[-k_d d_b (H-d) + k_\theta(\theta_1 - \theta_0)\right] \tag{3}$$

B. Friction force

Our new gripper has a new perching method called clipping, for which friction forces are utilized for perching onto objects with large height. To ensure successful clipping, it is necessary to analyze the friction force generated by the two contact feet for a perching object with a given size.

The clipping scenario is also depicted in Fig. 6, where a rectangular purple object is placed vertically with the contact feet clipping on it. We assume the surface of the perching object is flat and in the vertical direction. When the gripper is closed, its fingers will contact the surfaces to generate a normal force F_n, resulting in a friction force f that acts on the

1083-4435 (c) 2020 IEEE. Personal use is permitted, but republication/redistribution requires IEEE permission. See http://www.ieee.org/publications_standards/publications/rights/index.html for more information.
Authorized licensed use limited to: COLORADO STATE UNIVERSITY. Downloaded on July 26,2021 at 17:17:17 UTC from IEEE Xplore. Restrictions apply.

This article has been accepted for publication in a future issue of this journal, but has not been fully edited. Content may change prior to final publication. Citation information: DOI 10.1109/TMECH.2020.3037303, IEEE/ASME Transactions on Mechatronics

contact point to support the MAV's weight. a_3 is the distance from the beam pivot to the contact point, and φ is the angle between the horizontal direction and a_3 (Fig. 6). a_3 can be solved based on the geometric relationship shown in Fig. 5.

$$a_3 = \sqrt{a_1^2 + a_2^2 - 2a_1a_2\cos\alpha} \tag{4}$$

φ can also be solved similarly based on the geometric relationship shown in Fig. 6.

$$\varphi = \pi - \arccos\frac{a_1^2 + a_3^2 - a_2^2}{2a_1a_3} - \theta_1 \tag{5}$$

For a given design of the gripper, the size of the perching object can determine whether the perching is successful or not. Therefore, we need to solve the range of sizes for the object that will allow for successful perching. To do this, we first derive the vertical displacement d for the switching pad given the object's size P. Then, we obtain the normal force F_n from d. Finally, we can determine successful perching by checking if $\mu F_n \geq f = mg/2$, where μ is the friction coefficient, m is the mass of the MAV.

The relationship between the object size P and the displacement d can be obtained from the geometrical relationship (Fig. 6)

$$P = 2\left(d_b + L_0 + d_h - a_3\cos\varphi\right) \tag{6}$$

where $d_h = [(1-\gamma)l_t + l_h]\cos\theta_0$. From this equation, we can numerically solve d given P since d_b and φ are functions of d. To obtain the normal force F_n from d, we analyze the statics using free body diagram for fingers of the gripper. As shown in Fig. 6, there are four torques acting on the finger: recovering torque from the tube in clockwise direction τ_θ, torque generated by F_d from linear spring acting on tube pivot τ_{k_d} in clockwise direction, torque generated from F_n in counter-clockwise direction τ_{F_n}, and torque generated by f in counter-clockwise direction τ_f. If we assume MAV is able to perch on the object, i.e., $f = mg/2$. Then, we can have the torque equilibrium equation

$$\tau_{F_n} + \tau_f = \tau_\theta + \tau_{k_d} \tag{7}$$

By solving equation (7), the normal force F_n can be obtained as a function of d

$$F_n(d) = \frac{k_d d_b(H-d) + k_\theta(\theta_0 - \theta_1) - mg(d_h - P/2)/2}{a_3 sin\varphi + H - d} \tag{8}$$

With $F_n(d)$, we can see if the clipping perching will be successful by checking if $\mu F_n \geq f = mg/2$.

C. Bistability analysis

If the parameters in equation (3) are not chosen appropriately, the mechanism may become monostable, meaning it only has one stable state. To provide design guidelines to generate the bistability required for perching, we investigate how two important design parameters will influence the bistability of this mechanism.

We first qualitatively investigate the reason for bistability using simulations. The bistability of the designed gripper is generated by the competition of potential energy from the tubes (E_t) and beams (E_b). To see this, we plot E_t and E_b as well as the total energy (E) for a bistable (Fig. 7(a)) and monostable case (Fig. 7(b)). From the two figures, E_t will monotonically increase because the tube will increasingly bend as the displacement increases. But E_b will increase first and then decrease because d_b (Fig. 6) will first increase and then decrease. Combining E_t and E_b, the total energy $E = E_t + E_b$ can have either a single minimum at the initial configuration ($d = 0$, Fig. 7(b)) or two minima (Fig. 7(a)), with different choices of k_d and k_θ. Note that different k_d can be realized by choosing different thicknesses for the beam, while different k_θ can be achieved using tubes with different lengths.

In addition to the potential energy, we can also determine the bistable or monostable from the force-displacement characteristic. In the quasi-static state transition case, the force-displacement in Eqn. (3) is the first-order derivative of the potential energy, which can tell the direction of the potential energy curve. If the force is always positive, the energy will be monotonically increasing as in the monostable case (Fig. 7(b)). If the initial positive force becomes negative at some d, the potential energy will decrease and have a local minimum as in the bistable case (Fig. 7(a)). In other words, the system is bistable if there exists negative force in Eqn. (3) and monostable if $F \geq 0$ for all d.

With the observations for the force, we define a bistability index denoted as BI to numerically investigate how k_d and k_θ will influence the bistability

$$BI = -\frac{F_{min}}{F_{max}} \tag{9}$$

where F_{min} and F_{max} is the minimum and maximum force in the force-displacement characteristic of the bistable mechanism, respectively. For the gripper, $0 \leq BI \leq 1$. $BI = 0$ for all monostable mechanism since $F_{min} = 0$ at the initial configuration. $BI \leq 1$ means the magnitude of F_{min} is less or equal than F_{max}. This can be explained by looking at the slope of the energy curve. Because the decreasing of energy is only generated by E_b, the negative slope cannot be larger than the positive slope. The extreme case $BI = 1$ happens when $k_\theta = 0$, which means the tube is a traditional rotational joint without any torsional stiffness. This case will be the one illustrated in Fig. 2.

To systematically explore how will k_d and k_θ influence the bistability, we plot BI with respect to k_d and k_θ as shown in Fig. 7(c). In the simulation, we have $k_d \in [0, 5000]$ with a step size of 50 N/m and $k_\theta \in [0, 0.1]$ with a step size of 0.001 Nm/rad. The plot indicates that larger k_d will increase the bistability index because E_b will dominate E_t, making the shape of the total energy closer to E_b with two minima (Fig. 7(a)). Larger k_θ will decrease the bistability index, because E_t will dominate E_b, making the shape of the total energy closer to E_t with a single minimum.

IV. Experiment

In this section, we detail the fabrication of the gripper and experimentally test the force-displacement characteristic and compare it with the theoretical results. We also verify the object sizes for successful perching using the clipping

1083-4435 (c) 2020 IEEE. Personal use is permitted, but republication/redistribution requires IEEE permission. See http://www.ieee.org/publications_standards/publications/rights/index.html for more information.
Authorized licensed use limited to: COLORADO STATE UNIVERSITY. Downloaded on July 26,2021 at 17:17:17 UTC from IEEE Xplore. Restrictions apply.

This article has been accepted for publication in a future issue of this journal, but has not been fully edited. Content may change prior to final publication. Citation information: DOI 10.1109/TMECH.2020.3037303, IEEE/ASME Transactions on Mechatronics

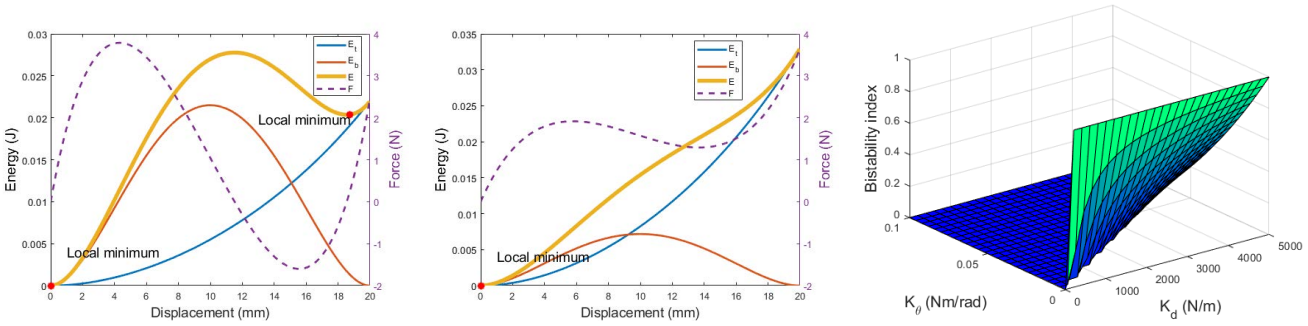

(a) (b) (c)

Fig. 7. Bistability analysis. (a) The gripper is bistable if $k_d = 3000N/m$ and $k_\theta = 0.02Nm/rad$. (b) the gripper is monostable if $k_d = 1000N/m$ and $k_\theta = 0.03Nm/rad$. (c) Bistability index will change with respect to k_d and k_θ.

method. Finally, perching experiments using both encircling and clipping methods are carried out on different objects in both controlled and uncontrolled environments.

A. Gripper fabrication and Perchflie

Most of the parts of the gripper are 3D-printed and then assembled. Five different parts (Fig. 4) are 3D-printed using veroclear material with an Objet printer (Objet30 pro, Stratasys): one base with two vertical beams and the motor enclosure, two fingers, one switching pad, two contact feet, and one level. The fingers are connected to the switching pad through a tube with an inner diameter of 1.5875 mm and an outer diameter of 6.35 mm (ULTRA-C-062-3, Sain-Tech). The film attached to the contact feet is fabricated from curable elastomers (Ecoflex30, Smooth-On). The DC motor (GH6124s, Gizmoszone) weighs less than 1.5 g and can provide 200 gcm torque. And the motor driver (DRV8838, Pololu) can provide a continuous current of 1.7 A with less than 1 g weight. The detailed design parameters for the gripper are shown in Table I. The parameters are chosen to make the gripper easy to close but stable to hold. With the design parameters, the theoretical switching forces for two directions are $F_{max} = 2.15$ N (opening force) and $F_{min} = -0.41$ N (closing force) respectively. The gripper system weighs about 8 g including the motor driver. It is then attached to the Crazyflie (Crazyflie2.0, Bitcraze) using a zip tie as shown in Fig. 8. The whole system, termed as Perchflie, is about 40 g including a flow deck on the bottom for stable motion control.

As shown in Fig. 4, the lever is connected to the stand with a shaft. The whole length of the lever is about 52 mm, of which both the pushing side and the dragging side is about 26 mm. With this dimension, the force and travel distance are the same for both sides. A string is coiled on the motor and the other side is tied to the dragging side of the lever. With this lever-motor system, a full opening procedure requires about 2 s at the full motor speed.

B. Force-displacement characteristic experiment

To verify our mathematical model that predicts the activation force, we first conduct experiments to obtain the force-displacement characteristic. The experiment setup is shown in Fig. 9. The main test machine is a motorized

Fig. 8. Perchflie. Gripper is attached to the Crazyflie with a zip tie. The whole system is about 40 g including a flow deck.

TABLE I
DESIGN PARAMETERS OF THE GRIPPER

$a_1(mm)$	$a_2(mm)$	$\alpha(^\circ)$	$\theta_0(^\circ)$	$h_b(mm)$
9	37.8	60	30	6.5
$l_b(mm)$	$l_f(mm)$	$l_t(mm)$	l_h(mm)	
23.8	15	6	8.81	

tension/compression test stand (ESM303, Mark-10). With a force gauge (M5-2, Mark-10) connected, the stand can move with a constant speed both upward and downward while measuring both tension and compression force. The measuring range of M5-2 is 10 N with a precision of 0.002 N. And a software (MESUR^{TM} gauge Plus, Mark-10) is used for recording the force and displacement data.

We separate the experiments into two parts to minimize possible hysteresis: dragging for the opening force and pushing for the closing force. In the dragging experiment, the gripper starts with the closed state and ends at $0N$ when no external force is needed to switch it to the open state. The switching pad is connected to the force gauge through a string. While the switching pad is dragged to move upward with a constant speed, the software records the displacement and force data. For the pushing experiment, the gripper starts with the open

1083-4435 (c) 2020 IEEE. Personal use is permitted, but republication/redistribution requires IEEE permission. See http://www.ieee.org/publications_standards/publications/rights/index.html for more information.
Authorized licensed use limited to: COLORADO STATE UNIVERSITY. Downloaded on July 26,2021 at 17:17:17 UTC from IEEE Xplore. Restrictions apply.

This article has been accepted for publication in a future issue of this journal, but has not been fully edited. Content may change prior to final publication. Citation information: DOI 10.1109/TMECH.2020.3037303, IEEE/ASME Transactions on Mechatronics

TABLE II
EXPERIMENT DATA AND SIMULATION DATA COMPARISON

	$F_{max}(N)$	$F_{min}(N)$	$d_o(mm)$	$d_c(mm)$
Simulation	2.15	-0.41	12.62	4.89
Experiment	2.12	-0.39	14.17	5.23
Error(%)	1.4	5.1	10.94	6.5

state and ends at 0 N when no external force is needed to switch it to the closed state. During the experiments, the force gauge moves downward to push the switching pad. 10 pushing and 10 dragging experiments are carried out, and the individual pushing and dragging experiment data is combined to generate a whole force-displacement characteristic figure. The experiment results are plotted in Fig. 10. The yellow shaded area shows the distribution range (maximum and minimum force at each displacement) of the experiment result. The dashed red line is the theoretical result, and the solid blue line shows the mean value of the 10 combined experiment results. To quantify the experiment results, there are several important parameters, i.e., maximum force F_{max}, minimum force F_{min}, maximum opening displacement d_o (displacement between the first two zero forces), and maximum closing displacement d_c (displacement between the last two zero forces). We show the mean of these 4 parameters in 10 experiments together with the theoretical value from the simulation in Table II.

From Fig. 10 and Table II, the experimental results are reasonably accurate. The error mainly comes from our simplified models. First, we model the beams as linear springs and the tubes as torsional springs, but they may not exactly follow the spring laws. Second, the fabrication and assembly process may also introduce some errors for the exact dimensions for each of the components. From Fig. 10, the error increases when the opening force is decreasing for the opening experiment. The largest error (10.94%) occurs with the maximum opening displacement. The reason is that the tubes are compressed since they are parallel to the base. This period corresponds to the lagging part of the experiment results. The compression will result in a smaller l_t, which will increase the bending stiffness K_θ based on PRBM. As analyzed in section III, larger K_θ will increase BI and make the system less bistable. This will make the force-displacement characteristic decrease more slowly. To better illustrate this phenomenon, we simulate several cases with six different tube lengths (5 mm to 7 mm with a step size of 0.4 mm) and plot the force-displacement characteristics to compare the difference (Fig. 11). The simulation results show that the force-displacement characteristics are almost the same before 9 mm displacement. After 9 mm, grippers with longer tubes tend to have a larger force to make the system more bistable. As a result, the force profiles for grippers with shorter tubes decrease slower than the longer ones, which explains the lagging of the experiment results.

C. Friction test experiment

As the gripper can generate different normal forces F_n and friction forces f on different sized objects, we experimentally test the prediction for successful perching on objects with different sizes in this subsection.

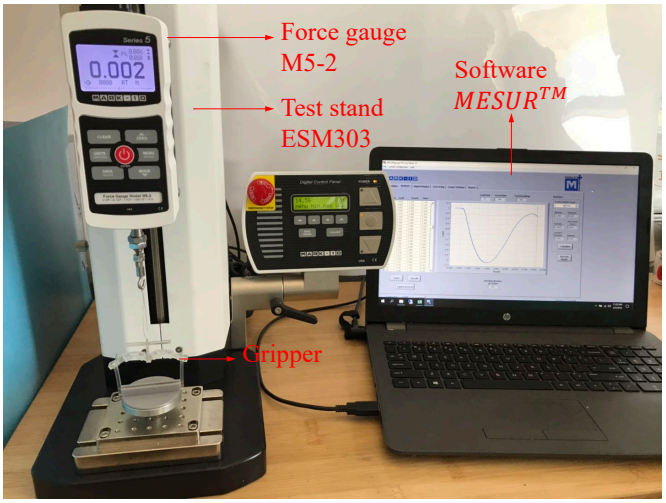

(a)

Fig. 9. Force-displacement characteristic experiment setup. The gripper is attached to the test stand and a hook is attached to the force gauge. In dragging experiment, the hook will pull the switching pad with a string. In pushing experiment, the hook will directly push the switching pad. Meanwhile, the software will record the corresponding displacement and tension/compression force.

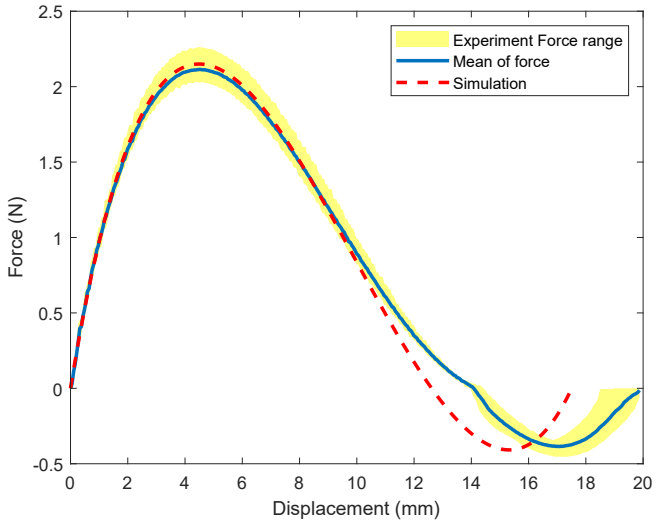

Fig. 10. Force-displacement characteristic experiment results. 10 pushing and 10 dragging experiments are carried out. The yellow shaded area shows the experiment force range. The blue line shows the mean of forces from 10 experiments. The dashed red line shows the simulation result from mathematical models.

We use 3D printed objects made from Polylactic Acid (PLA) with different sizes as the perching object. First, we experimentally test the friction coefficient μ between Ecoflex 30 and 3D printed PLA. Since Ecoflex 30 is soft, the friction coefficient between it and PLA is not constant. We experimentally test and find that the friction coefficient varies with normal force. In this experiment, we designed a container with a mass of 3.08 g. Then we added different weights from 0 g to 65 g with a step size of 5 g, and use the test stand to horizontally drag the ecoflex 30 on 3D printed PLA surface. The maximum friction force before relative motion occurs is recorded to calculate μ. After 6 consistent tests, we find that

1083-4435 (c) 2020 IEEE. Personal use is permitted, but republication/redistribution requires IEEE permission. See http://www.ieee.org/publications_standards/publications/rights/index.html for more information.
Authorized licensed use limited to: COLORADO STATE UNIVERSITY. Downloaded on July 26,2021 at 17:17:17 UTC from IEEE Xplore. Restrictions apply.

This article has been accepted for publication in a future issue of this journal, but has not been fully edited. Content may change prior to final publication. Citation information: DOI 10.1109/TMECH.2020.3037303, IEEE/ASME Transactions on Mechatronics

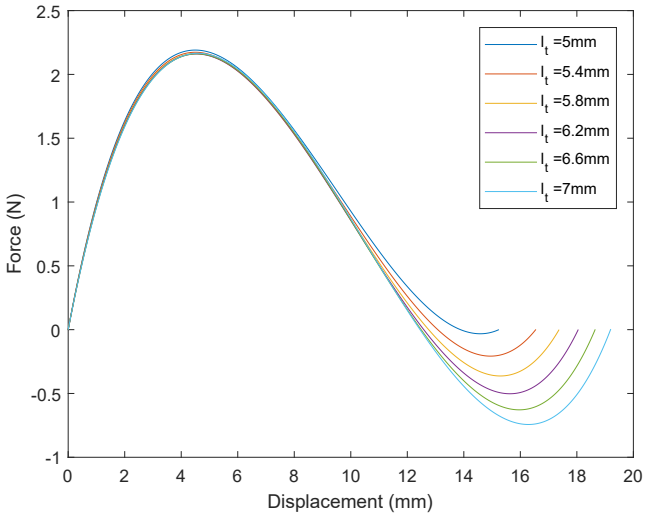

Fig. 11. Simulations for the influence of different tube length to the force-displacement characteristic. Six different tube lengths from 5 mm to 7 mm are used. For different tube lengths, the force-displacement characteristics are almost the same before about 9 mm displacement. After 9 mm, the gripper with longer tubes tends to have a larger recover force to make the system more bistable.

a minimum of 5th order polynomial can fit the result well:

$$\mu = -52{F_n}^5 + 107{F_n}^4 - 80{F_n}^3 + 27{F_n}^2 - 4F_n + 1 \quad (10)$$

With Eqn. (8) and Eqn. (10), we can calculate the range for the size of the PLA objects that will allow for successful perching. The perching object should have a width from 3.7 mm to 36.4 mm.

To verify the prediction, we printed several PLA cubes with eight different sizes for boundary cases: 3, 4, 5, 6, 33, 34, 35, and 36 mm. We manually make the robot clip on the cubes and see whether it can stay or not. The results show that the robot can perch on such cubes with sizes of 5, 6, and 33 mm, which is a bit smaller than the estimation range. This error might be caused by the friction coefficient estimation.

D. Perching and grasping experiment

After verifying our models, we conduct various perching experiments for Perchflie in controlled and uncontrolled environments as well as the grasping experiment. For encircling perching, as long as the dimension of the perching object is smaller than the space formed by the fingers and switching pad, the Perchflie can successfully perch on it. For tall objects, the robot can use the clipping method to clip on the objects to hold the Perchflie with enough friction forces.

The perching experiments are conducted on two different objects with the two perching methods: encircling and clipping, with two typical experiments shown as image sequences in Fig. 12. The clipping perching is conducted on a vertically placed cardboard with a width of 7 mm. The encircling perching is conducted on a cuboid wood with a width of 31 mm and a height of 5 mm. In each experiment, the Perchflie is manually controlled to take off and accelerate to the perching object. With an impact force acting on the switching pad, the gripper will close to perch with either clipping or encircling method. After perching, the motor is controlled to open the gripper. After detachment, Perchflie hovers immediately. The motor continues rotation to fully open the gripper while hovering. After the gripper is fully opened, the motor will rotate in the opposite direction to leave the lever away from the switching pad for the next perching. At last, the motor stops and Perchflie can perch again. Fig. 12 illustrates the perching sequence for one cycle of perching and releasing for the two different objects. Detailed motion for each perching is provided in a supplemental video.

Besides the controlled perching experiments, we also conduct two perching experiments in uncontrolled natural environments. The first perching experiment is conducted on a plastic pipe. The Perchflie is manually controlled to perch on the pipe with the encircling method. The second perching experiment is on a vertically placed poster board with the clipping method. In both experiments, the Perchflie can perch, release, and hover, as shown in the supplemental video.

To investigate the potential of this bistable gripper, we conducted one more grasping experiment. Limited by the payload of the Crazyflie, the object is a $116\times77\times14$ mm foam. The foam is manually put on the gripper when the Perchflie is airborne. After the Perchflie arrives at the destination. The gripper is controlled to release the object. The process is shown in Fig. 13. The detailed motion is provided in the supplemental video.

V. Conclusions and Future Work

In this paper, we design, analyze, and develop a bistable compliant gripper to enable passive perching for MAVs. With bistability, the gripper can passively switch from open to closed by impact forces to perch onto an object. With a level mechanism driven by a DC motor to open the gripper, it can detach from the object. It also provides two different perching methods, clipping and encircling, to expand the objects that it can perch. We investigate the cause of the bistability to provide a design guideline by defining a bistability index. We also establish a model to predict the force-displacement characteristic for the gripper and experimentally verify the proposed model. Various experiments are conducted to show the feasibility of this gripper for MAV perching and grasping.

Our future work will focus on two aspects: theoretical analysis and design improvements. For theoretical aspects, we will leverage better models (e.g., beam constraint model (BCM)) to investigate the bistable mechanism with compliant joints. The Pseudo-Rigid-Body-Model (PRBM) used in this paper assumes a constant characteristic radius (γl_t), which should vary with loading conditions, boundary conditions, or initial beam curvature [32]. To solve this problem, BCM will be implemented for more accurate force-displacement characteristic prediction. The design improvements will consist of two main parts. First, the current release mechanism (the motor-driven lever system) occupies a large 3D space, which can be improved using some in-plane mechanisms (e.g., a Sarrus linkage). Second, as observed from the experiments, during the release after encircling perching, the contact feet might interact with the perching objects, which needs some

1083-4435 (c) 2020 IEEE. Personal use is permitted, but republication/redistribution requires IEEE permission. See http://www.ieee.org/publications_standards/publications/rights/index.html for more information.
Authorized licensed use limited to: COLORADO STATE UNIVERSITY. Downloaded on July 26,2021 at 17:17:17 UTC from IEEE Xplore. Restrictions apply.

This article has been accepted for publication in a future issue of this journal, but has not been fully edited. Content may change prior to final publication. Citation information: DOI 10.1109/TMECH.2020.3037303, IEEE/ASME Transactions on Mechatronics

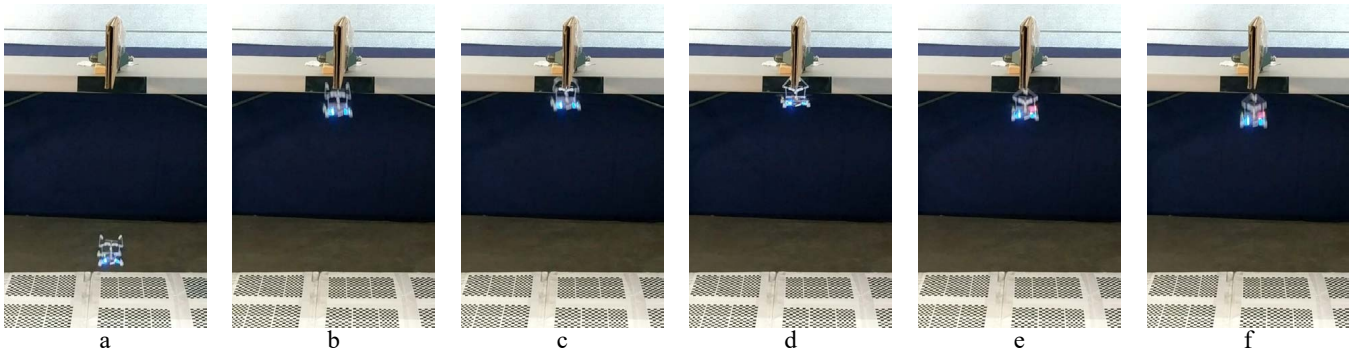

(a) Clipping perch

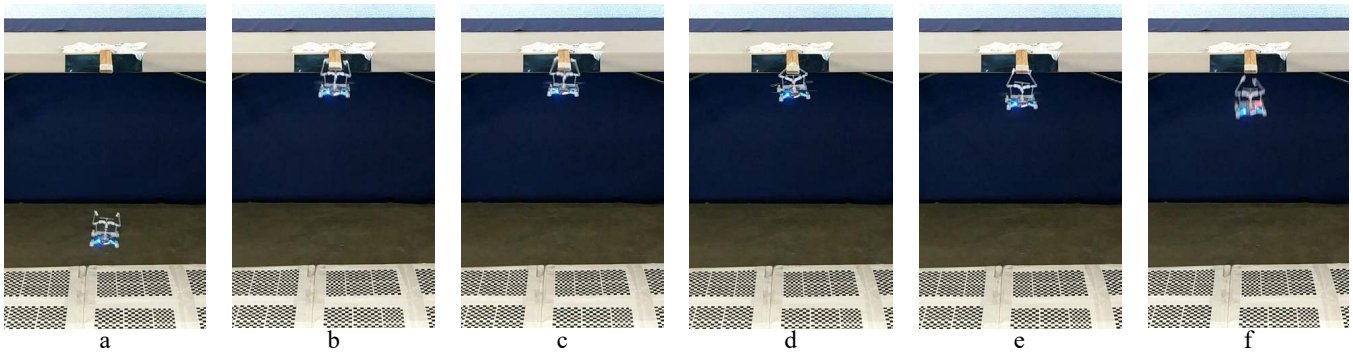

(b) Encircling perch

Fig. 12. Two perching experiments on different objects with two perching methods. The first image sequence shows the clipping method on cardboard. The second image sequence shows the encircling method. In each experiment, the Perchflie undergoes a) taking off, b-c) perching, d) staying on the object, e-f) releasing. A detailed view of the perching state for both clipping and encircling is shown in Fig. 1 (b) and (c).

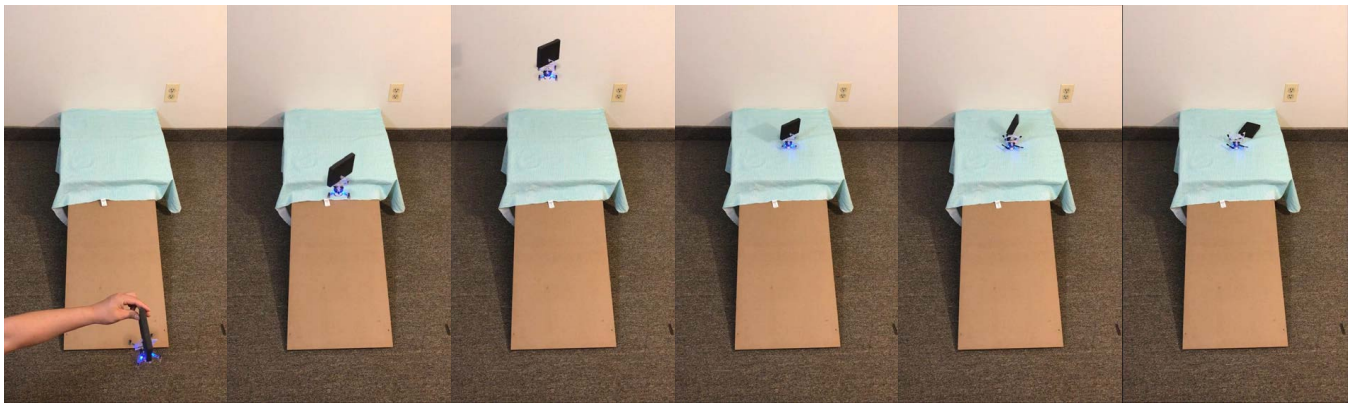

Fig. 13. Image sequence for aerial grasping. A foam is manually put on the gripper when the robot is airborne. After the Perchflie arrives at the destination, it lands and opens the gripper to release the foam.

maneuvers for a successful release. We will also revise the design of the contact feet to make releasing more smooth. Eventually, we aim to accomplish autonomous perching by synergistically integrating mechanical intelligence: the bistable gripper, with our previous work on computational intelligence: estimation, planning, and control algorithms.

ACKNOWLEDGMENT

This research is supported by National Science Foundation under grants IIS-1815476 and IIS-1815519

REFERENCES

[1] D. Floreano and R. J. Wood, "Science, technology and the future of small autonomous drones," *Nature*, vol. 521, no. 7553, p. 460, 2015.
[2] P. Liu, S. P. Sane, J.-M. Mongeau, J. Zhao, and B. Cheng, "Flies land upside down on a ceiling using rapid visually mediated rotational maneuvers," *Science advances*, vol. 5, no. 10, p. eaax1877, 2019.
[3] M. Kovac, "Learning from nature how to land aerial robots," *Science*, vol. 352, no. 6288, pp. 895–896, 2016.
[4] W. R. Roderick, D. D. Chin, M. R. Cutkosky, and D. Lentink, "Birds land reliably on complex surfaces by adapting their foot-surface interactions upon contact," *eLife*, vol. 8, 2019.
[5] H. Zhang and J. Zhao, "Vision based surface slope estimation for unmanned aerial vehicle perching," in *ASME 2018 Dynamic Systems and Control Conference*, pp. V002T21A004–V002T21A004, American Society of Mechanical Engineers, 2018.

1083-4435 (c) 2020 IEEE. Personal use is permitted, but republication/redistribution requires IEEE permission. See http://www.ieee.org/publications_standards/publications/rights/index.html for more information.
Authorized licensed use limited to: COLORADO STATE UNIVERSITY. Downloaded on July 26,2021 at 17:17:17 UTC from IEEE Xplore. Restrictions apply.

This article has been accepted for publication in a future issue of this journal, but has not been fully edited. Content may change prior to final publication. Citation information: DOI 10.1109/TMECH.2020.3037303, IEEE/ASME Transactions on Mechatronics

[6] H. Zhang, B. Cheng, and J. Zhao, "Optimal trajectory generation for time-to-contact based aerial robotic perching," *Bioinspiration & biomimetics*, vol. 14, no. 1, p. 016008, 2018.

[7] M. T. Pope, C. W. Kimes, H. Jiang, E. W. Hawkes, M. A. Estrada, C. F. Kerst, W. R. Roderick, A. K. Han, D. L. Christensen, and M. R. Cutkosky, "A multimodal robot for perching and climbing on vertical outdoor surfaces," *IEEE Transactions on Robotics*, vol. 33, no. 1, pp. 38–48, 2017.

[8] M. Graule, P. Chirarattananon, S. Fuller, N. Jafferis, K. Ma, M. Spenko, R. Kornbluh, and R. Wood, "Perching and takeoff of a robotic insect on overhangs using switchable electrostatic adhesion," *Science*, vol. 352, no. 6288, pp. 978–982, 2016.

[9] M. Anderson, "The sticky-pad plane and other innovative concepts for perching uavs," in *47th AIAA Aerospace Sciences Meeting Including The New Horizons Forum and Aerospace Exposition*, p. 40, 2009.

[10] L. Daler, A. Klaptocz, A. Briod, M. Sitti, and D. Floreano, "A perching mechanism for flying robots using a fibre-based adhesive," in *2013 IEEE International Conference on Robotics and Automation*, pp. 4433–4438, May 2013.

[11] M. Kovač, J. Germann, C. Hürzeler, R. Y. Siegwart, and D. Floreano, "A perching mechanism for micro aerial vehicles," *Journal of Micro-Nano Mechatronics*, vol. 5, no. 3-4, pp. 77–91, 2009.

[12] K. Zhang, P. Chermprayong, T. M. Alhinai, R. Siddall, and M. Kovac, "Spidermav: Perching and stabilizing micro aerial vehicles with bio-inspired tensile anchoring systems," in *2017 IEEE/RSJ International Conference on Intelligent Robots and Systems (IROS)*, pp. 6849–6854, Sep. 2017.

[13] D. Mehanovic, J. Bass, T. Courteau, D. Rancourt, and A. L. Desbiens, "Autonomous thrust-assisted perching of a fixed-wing uav on vertical surfaces," in *Conference on Biomimetic and Biohybrid Systems*, pp. 302–314, Springer, 2017.

[14] J. Thomas, M. Pope, G. Loianno, E. W. Hawkes, M. A. Estrada, H. Jiang, M. R. Cutkosky, and V. Kumar, "Aggressive flight with quadrotors for perching on inclined surfaces," *Journal of Mechanisms and Robotics*, vol. 8, no. 5, p. 051007, 2016.

[15] C. E. Doyle, J. J. Bird, T. A. Isom, J. C. Kallman, D. F. Bareiss, D. J. Dunlop, R. J. King, J. J. Abbott, and M. A. Minor, "An avian-inspired passive mechanism for quadrotor perching," *IEEE/ASME Transactions on Mechatronics*, vol. 18, pp. 506–517, April 2013.

[16] H. Nguyen, R. Siddall, B. Stephens, A. Navarro-Rubio, and M. Kovač, "A passively adaptive microspine grapple for robust, controllable perching," in *2019 2nd IEEE International Conference on Soft Robotics (RoboSoft)*, pp. 80–87, April 2019.

[17] K. Hang, X. Lyu, H. Song, J. A. Stork, A. M. Dollar, D. Kragic, and F. Zhang, "Perching and resting—a paradigm for uav maneuvering with modularized landing gears," *Science Robotics*, vol. 4, no. 28, p. eaau6637, 2019.

[18] L. L. Howell, *Compliant mechanisms*. John Wiley & Sons, 2001.

[19] T.-A. Nguyen and D.-A. Wang, "A gripper based on a compliant bitable mechanism for gripping and active release of objects," in *Manipulation, Automation and Robotics at Small Scales (MARSS), International Conference on*, pp. 1–4, IEEE, 2016.

[20] T. G. Thuruthel, S. H. Abidi, M. Cianchetti, C. Laschi, and E. Falotico, "A bistable soft gripper with mechanically embedded sensing and actuation for fast closed-loop grasping," *arXiv preprint arXiv:1902.04896*, 2019.

[21] T. Chen, J. Mueller, and K. Shea, "Integrated design and simulation of tunable, multi-state structures fabricated monolithically with multi-material 3d printing," *Scientific reports*, vol. 7, p. 45671, 2017.

[22] J.-S. Koh, E. Yang, G.-P. Jung, S.-P. Jung, J. H. Son, S.-I. Lee, P. G. Jablonski, R. J. Wood, H.-Y. Kim, and K.-J. Cho, "Jumping on water: Surface tension–dominated jumping of water striders and robotic insects," *Science*, vol. 349, no. 6247, pp. 517–521, 2015.

[23] T. Chen, O. R. Bilal, K. Shea, and C. Daraio, "Harnessing bistability for directional propulsion of soft, untethered robots," *Proceedings of the National Academy of Sciences*, p. 201800386, 2018.

[24] J. A. Faber, A. F. Arrieta, and A. R. Studart, "Bioinspired spring origami," *Science*, vol. 359, no. 6382, pp. 1386–1391, 2018.

[25] P. Rothemund, A. Ainla, L. Belding, D. J. Preston, S. Kurihara, Z. Suo, and G. M. Whitesides, "A soft, bistable valve for autonomous control of soft actuators," *Science Robotics*, vol. 3, no. 16, p. eaar7986, 2018.

[26] A. Alqasimi, C. Lusk, and J. Chimento, "Design of a linear bistable compliant crank–slider mechanism," *Journal of Mechanisms and Robotics*, vol. 8, no. 5, p. 051009, 2016.

[27] Q.-D. Truong, D.-A. Wang, *et al.*, "Design and characterization of a mouse trap based on a bistable mechanism," *Sensors and Actuators A: Physical*, vol. 267, pp. 360–375, 2017.

[28] B. Haghpanah, L. Salari-Sharif, P. Pourrajab, J. Hopkins, and L. Valdevit, "Multistable shape-reconfigurable architected materials," *Advanced Materials*, vol. 28, no. 36, pp. 7915–7920, 2016.

[29] H. Zhang, J. Sun, and J. Zhao, "Compliant bistable gripper for aerial perching and grasping," in *2019 International Conference on Robotics and Automation (ICRA)*, pp. 1248–1253, IEEE, 2019.

[30] J. Sun and J. Zhao, "An adaptive walking robot with reconfigurable mechanisms using shape morphing joints," *IEEE Robotics and Automation Letters*, vol. 4, no. 2, pp. 724–731, 2019.

[31] A. DeMario and J. Zhao, "Development and Analysis of a Three-Dimensional Printed Miniature Walking Robot With Soft Joints and Links," *Journal of Mechanisms and Robotics*, vol. 10, 04 2018.

[32] S. Awtar and S. Sen, "A generalized constraint model for two-dimensional beam flexures: nonlinear load-displacement formulation," *Journal of Mechanical Design*, vol. 132, no. 8, 2010.

Haijie Zhang Haijie Zhang received the B.S. degree from the School of Automation, Harbin Engineering University, Harbin, P.R. China, in 2014. He is currently working toward the Ph.D. degree in the Adaptive Robotics Lab at Colorado State University, Fort Collins, CO, USA. His research interests include vision based control and flying robots.

Elisha Lerner is currently working toward a B.S. degree in mechanical engineering from Colorado State University and intends to graduate in the spring of 2021. He currently works in the Adaptive Robotics Lab at Colorado State University, Fort Collins. His research includes mechanical grasping and robotics.

Bo Cheng received the B.S. degree in automation from Zhejiang University, Hangzhou, China, in 2006, the M.S. degree in mechanical engineering from the University of Delaware, Newark, DE, USA, in 2009, and the Ph.D. degree in mechanical engineering from Purdue University, West Lafayette, IN, USA, in 2012. He is currently an Associate Professor and Kenneth K. and Olivia J. Kuo Early Career Professor at the Department of Mechanical Engineering, Pennsylvania State University, University Park, PA, USA. His research interests include biologically inspired robotics, animal flight, fish swimming, and robot control and learning.

Jianguo Zhao received the B.E. degree in Mechanical Engineering from Harbin Institute of Technology, Harbin, China and M.E. degree in Mechatronic Engineering from Shenzhen Graduate School, Harbin Institute of Technology, Shenzhen, China, in 2005 and 2007, respectively. He received his Ph.D. degree in Electrical Engineering from Michigan State University, East Lansing, Michigan, USA, in 2015.

He is currently an Assistant Professor at Colorado State University and the director of Adaptive Robotics Lab. His research interests include bio-inspired robotics, dynamics and control, and vision based control.

1083-4435 (c) 2020 IEEE. Personal use is permitted, but republication/redistribution requires IEEE permission. See http://www.ieee.org/publications_standards/publications/rights/index.html for more information.
Authorized licensed use limited to: COLORADO STATE UNIVERSITY. Downloaded on July 26,2021 at 17:17:17 UTC from IEEE Xplore. Restrictions apply.